Numerical Analysis and Scientific Computing
Preprint Seria

A finite element method for the Navier-Stokes equations in moving domain with application to hemodynamics of the left ventricle

A. Danilov A. Lozovskiy M. A. Olshanskii
Yu. V. Vassilevski

Preprint #60

Department of Mathematics
University of Houston

May 2017

A finite element method for the Navier-Stokes equations in moving domain with application to hemodynamics of the left ventricle*

Alexander Danilov † Alexander Lozovskiy‡ Maxim A. Olshanskii§
Yuri V. Vassilevski¶

Abstract

The paper introduces a finite element method for the Navier-Stokes equations of incompressible viscous fluid in a time-dependent domain. The method builds on a quasi-Lagrangian formulation of the problem and handles geometry in a time-explicit way. We prove that numerical solution satisfies a discrete analogue of the fundamental energy estimate. This stability estimate does not require a CFL time-step restriction. The method is further applied to simulate a flow in a model of the left ventricle of a human heart, where the ventricle wall dynamics is reconstructed from a sequence of contrast enhanced Computed Tomography images.

1 Introduction

Fluid flows in time-dependent domains are ubiquitous in nature and engineering. In many cases, fluid–structure interaction phenomena play important role and the domain evolution is an unknown in the mathematical model that couples fluid and structure dynamics. Examples include blood flow in compliant vessels, flows around turbine blades or fish locomotion. In other situations, one may assume that the motion of the domain is given and one has to recover the induced fluid flow. In biomedical applications, this second scenario is often accepted for the blood flow simulations in a human heart when the (patient-specific) motion of the heart walls is recovered from a sequence of Magnetic Resonance (MR), contrast enhanced Computed Tomography (ceCT) or ultrasonic images, see, e.g., [1–8]. Nowadays numerical simulations are commonly used to understand fluid dynamics and predict statistics of practical interest in this and other applications. In the conventional approach one considers the Navier-Stokes equations in a time-dependent domain to describe the fluid dynamics and further applies numerical method to solve them. In the present paper, we introduce a finite element (FE) method for a quasi-Lagrangian formulation of the incompressible Navier-Stokes equations in a moving domain. We analyze its numerical stability, and apply the method to simulate a flow in a model of the left ventricle of a human heart.

*This work has been supported by the Russian Science Foundation (RSF) grant 14-31-00024.

†Institute of Numerical Mathematics RAS and Moscow Institute of Physics and Technology; a.a.danilov@gmail.com

‡Institute of Numerical Mathematics RAS; saiya-jin@yandex.ru

§Department of Mathematics, University of Houston; molshan@math.uh.edu

¶Institute of Numerical Mathematics RAS and Moscow Institute of Physics and Technology; yuri.vassilevski@gmail.com

Several techniques have been introduced in the literature to overcome the numerical difficulties due to the evolution of the domain. This includes the space–time finite element formulations, immersed boundary methods, level-set method, fictitious domain method, unfitted finite elements, and arbitrary Lagrangian–Eulerian (ALE) formulation, see, e.g., [9–17]. In this paper we propose a finite element method based on a quasi-Lagrangian formulation of the equations in the reference domain. The method uses a fixed mesh fitted to the boundary of the computational domain. The time-dependent coefficients, which account for the domain evolution, are handled with a time lag. This and the linearization of the inertia terms lead to a *linear* discrete problem on each time step. We prove the stability of this semi-explicit method without any CFL-type restriction on the time-step. Related analyses of finite element methods for parabolic or fluid equations in moving domains can be found in several places in the literature. We note that well-posedness of space-time weak saddle-point formulations of the (Navier–)Stokes equations is a subtle question, see the recent treatment in [18] for the case of a steady domain. This may explain why a rigorous stability and convergence analysis of space–time (FE) methods for fluid problems is seemingly lacking. Scalar problems are understood much better; for example, a space–time discontinuous FE method for advection–diffusion problems on time-dependent domains was analyzed in [19]. ALE and Lagrangian finite element methods are more amenable to analysis. The stability of ALE finite element methods for parabolic evolution problems was treated in [16]. In [20] the authors analyzed the convergence of a finite element ALE method for the Stokes equations in a time-dependent domain when the motion of the domain is given. The analysis imposes time step restriction and certain smoothness assumptions for the finite element displacement field. In the present paper, we prove the energy stability of a finite element method applied to the quasi-Lagrangian formulation of the Navier-Stokes problem.

We further illustrate the performance of the numerical method by applying it to simulate a flow dynamics in a model of the human left ventricle. The domain motion in this example is reconstructed from a sequence of ceCT images of a real patient heart over one cardiac cycle. Several techniques are commonly used for dynamic model reconstruction from medical images, including control points tracking [1, 4] and contour propagation [3, 5]. In some cases, the conventional thresholding method is sufficient, in others, the manual segmentation is required. In our work, we use machine learning technique trained on partial manual segmentation. The details of the reconstruction method and results of the simulation are given in section 5.

2 Mathematical model

Consider a time-dependent domain $\Omega(t) \subset \mathbb{R}^d$, $d = 2, 3$, occupied by fluid. To formulate a flow problem, we introduce the reference domain $\Omega_0 = \Omega(0)$ and a mapping from the space–time cylinder $Q := \Omega_0 \times [0, T]$ to the physical domain,

$$\boldsymbol{\xi} \ : \ Q \to \bigcup_{t\in[0,T]} \Omega(t).$$

The mapping is assumed to be level-preserving, i.e. $\boldsymbol{\xi}(\Omega_0 \times \{t\}) = \Omega(t)$ for all $t \in [0, T]$. We assume also that the evolution of $\Omega(t)$ is sufficiently smooth such that $\boldsymbol{\xi} \in C^2(Q)^d$. Denote the spatial gradient matrix of $\boldsymbol{\xi}$ by $\mathbf{F} = \nabla_{\mathbf{x}}\boldsymbol{\xi}$, and $J := \det(\mathbf{F})$. Furthermore, we assume that there exist such positive reals C_F, c_J that

$$\inf_Q J \geq c_J > 0, \quad \sup_Q(\|\mathbf{F}\|_F + \|\mathbf{F}^{-1}\|_F) \leq C_F, \quad \text{with } \|\mathbf{F}\|_F := \mathrm{tr}(\mathbf{F}\mathbf{F}^T)^{\frac{1}{2}}. \tag{1}$$

The dynamics of incompressible Newtonian fluid can be described in terms of the velocity vector field $\hat{\mathbf{u}}(\mathbf{x},t)$ and the pressure function $\hat{p}(\mathbf{x},t)$ defined in $\Omega(t)$ for $t\in[0,T]$. In this paper, we distinguish between the no-slip $\partial\Omega^{ns}(t)$, Dirichlet $\partial\Omega^{D}(t)$ and outflow $\partial\Omega^{N}(t)$ parts of the boundary, and $\partial\Omega(t)=\partial\Omega^{ns}(t)\cup\partial\Omega^{D}(t)\cup\partial\Omega^{N}(t)$. On $\partial\Omega^{ns}(t)$ we impose no-penetration no-slip boundary condition, i.e. the fluid velocity on $\partial\Omega(t)$ is equal to the material velocity of the boundary (see Remark 1 below),

$$\hat{\mathbf{u}}=\boldsymbol{\xi}_t\circ\boldsymbol{\xi}^{-1}\quad\text{on }\partial\Omega^{ns}(t), \tag{2}$$

while on $\partial\Omega^{D}(t)$ and $\partial\Omega^{N}(t)$ we prescribe Dirichlet and Neumann conditions,

$$\hat{\mathbf{u}}=\hat{\mathbf{u}}_D\quad\text{on }\partial\Omega^{D}(t),\quad \widehat{\boldsymbol{\sigma}}\mathbf{n}=\hat{\mathbf{g}}\quad\text{on }\partial\Omega^{N}(t). \tag{3}$$

Here $\mathbf{u}_D$ is a given velocity, $\widehat{\boldsymbol{\sigma}}$ denotes the Cauchy stress tensor, and $\mathbf{n}$ is the exterior unit normal vector on $\partial\Omega^{N}(t)$.

Remark 1. The normal velocity of the boundary $\partial\Omega(t)$ is $v_\Gamma=\mathbf{n}\cdot(\boldsymbol{\xi}_t\circ\boldsymbol{\xi}^{-1})$. However, the material tangential velocity of the boundary is defined by the tangential part of $\boldsymbol{\xi}_t$ only if $\boldsymbol{\xi}$ is the Lagrangian mapping, i.e. $\boldsymbol{\xi}(\mathbf{x},t)$, $t\in[0,T]$, defines the material trajectory for $\mathbf{x}\in\Omega_0$ (or at least for $\mathbf{x}\in\partial\Omega_0$). In some applications such Lagrangian mapping is not available, and in this case (2) may produce spurious tangential velocities on the boundary. Thus, in practice one may amend (2) based on any additional information about the tangential motions for a better model.

This paper introduces a finite element method for fluid equations formulated in the reference domain. For $\mathbf{u}=\hat{\mathbf{u}}\circ\boldsymbol{\xi}$, $p=\hat{p}\circ\boldsymbol{\xi}$ defined in Q, the fluid dynamics is given by the following set of equations:

$$\begin{cases}\mathbf{u}_t-J^{-1}\mathrm{div}\,(J(\widehat{\boldsymbol{\sigma}}\circ\boldsymbol{\xi})\mathbf{F}^{-T})+(\nabla\mathbf{u})(\mathbf{F}^{-1}(\mathbf{u}-\boldsymbol{\xi}_t))=\mathbf{f}\\ \qquad\qquad\qquad\qquad\qquad\qquad\mathrm{div}\,(J\mathbf{F}^{-1}\mathbf{u})=0\end{cases}\quad\text{in }\ Q, \tag{4}$$

with body forces $\mathbf{f}=\hat{\mathbf{f}}\circ\boldsymbol{\xi}$. The governing equations are complemented with the initial condition

$$\mathbf{u}(\mathbf{x},0)=\mathbf{u}_0(\mathbf{x})\ \text{ in }\Omega_0. \tag{5}$$

We assume the fluid to be Newtonian, with the kinematic viscosity parameter ν. The constitutive relation in the reference domain reads

$$\widehat{\boldsymbol{\sigma}}\circ\boldsymbol{\xi}=-p\mathbf{I}+\nu(\nabla\mathbf{u}\mathbf{F}^{-1}+\mathbf{F}^{-T}(\nabla\mathbf{u})^T)\quad\text{in }Q. \tag{6}$$

The solvability of the problem (4) and the existence of its weak solutions is treated, for example, in [21]. Moreover, it is shown in [21] that for smoothly evolving $\Omega(t)$ the mapping $\boldsymbol{\xi}$ can be chosen in such a way that J depends only on t. However, from numerical viewpoint, such a mapping $\boldsymbol{\xi}$ may not be practically available, and so we allow J to vary in time and space.

Before recalling the energy balance for a smooth solution of the fluid problem, we recall a few useful identities. The mass balance yields the equality

$$J_t+\mathrm{div}\,(J\mathbf{F}^{-1}(\mathbf{u}-\boldsymbol{\xi}_t))=0\quad\text{in }Q. \tag{7}$$

The Piola identity, $\mathrm{div}\,(J\mathbf{F}^{-1})=0$, implies the following equality

$$\mathrm{div}\,(J\mathbf{F}^{-1}\mathbf{u})=J(\nabla\mathbf{u}):\mathbf{F}^{-T}\quad\text{in }Q, \tag{8}$$

where $\mathbf{A}:\mathbf{B}:=\mathrm{tr}(\mathbf{A}\mathbf{B}^T)$.

2.1 Energy equality

For the analysis, we shall assume that no-penetration no-slip boundary condition (2) is imposed on the whole boundary, i.e. $\partial\Omega(t) = \partial\Omega^{ns}(t)$. We handle non-homogeneous boundary conditions in a standard way using the decomposition $\mathbf{u} = \mathbf{v} + \mathbf{v}_1$, with $\mathbf{v}_1 = \boldsymbol{\xi}_t$ on $\partial\Omega_0 \times [0,T]$. Moreover, there exists $\mathbf{v}_1 \in C^1(Q)^d$ satisfying $\operatorname{div}(J\mathbf{F}^{-1}\mathbf{v}_1) = 0$, cf. [21]. From this, the continuity equation in (4), and boundary condition (2), it follows that

$$\operatorname{div}(J\mathbf{F}^{-1}\mathbf{v}) = 0 \quad \text{and} \quad \mathbf{v} = 0 \ \text{ on } \partial\Omega_0 \times [0,T]. \tag{9}$$

By $(\cdot,\cdot)$ we denote the $L^2(\Omega_0)$ scalar product, and $\|\cdot\|$ denotes the $L^2(\Omega_0)$ norm. For vector fields $\mathbf{v}, \mathbf{u} : \Omega_0 \to \mathbb{R}^d$ and tensor fields $\mathbf{A}, \mathbf{B} : \Omega_0 \to \mathbb{R}^{d\times d}$, we use the same notation to denote $(\mathbf{u},\mathbf{v}) = \int_{\Omega_0} \mathbf{u}^T\mathbf{v}\,\mathrm{d}\mathbf{x}$ and $(\mathbf{A},\mathbf{B}) = \int_{\Omega_0} \operatorname{tr}(\mathbf{A}\mathbf{B}^T)\,\mathrm{d}\mathbf{x}$, and obviously $\|\mathbf{u}\| := (\mathbf{u},\mathbf{u})^{\frac{1}{2}}$, $\|\mathbf{A}\| := (\mathbf{A},\mathbf{A})^{\frac{1}{2}}$. We make use of the identity:

$$(\mathbf{w}\cdot\nabla u, v) + \frac{1}{2}((\operatorname{div}\mathbf{w})u, v) = \frac{1}{2}\left((\mathbf{w}\cdot\nabla u, v) - (\mathbf{w}\cdot\nabla v, u)\right) + \frac{1}{2}\int_{\partial\Omega_0} (\mathbf{n}\cdot\mathbf{w})uv\,\mathrm{d}\mathbf{s}. \tag{10}$$

We multiply the first equality in (4) by $\mathbf{v}$, integrate it over the reference domain, and employ (10) for integration by parts and cancellation of the pressure term. We get

$$\begin{aligned}\frac{1}{2}\frac{d}{dt}\|J^{\frac{1}{2}}\mathbf{v}\|^2 - \frac{1}{2}(J_t\,\mathbf{v},\mathbf{v}) - (J(\boldsymbol{\sigma}\circ\boldsymbol{\xi})\mathbf{F}^{-T}, \nabla\mathbf{v}) \\ + \frac{1}{2}(\operatorname{div}(J\mathbf{F}^{-1}(\mathbf{v}-\boldsymbol{\xi}_t))\,\mathbf{v},\mathbf{v}) + (J(\nabla\mathbf{v}_1\mathbf{F}^{-1}\mathbf{v}),\mathbf{v}) \\ = (J\mathbf{f},\mathbf{v}) - \left(J\frac{\partial\mathbf{v}_1}{\partial t},\mathbf{v}\right) - (J(\nabla\mathbf{v}_1)(\mathbf{F}^{-1}(\mathbf{v}_1-\boldsymbol{\xi}_t)),\mathbf{v}).\end{aligned}$$

The identity (7) leads to some cancellations and we get

$$\begin{aligned}\frac{1}{2}\frac{d}{dt}\|J^{\frac{1}{2}}\mathbf{v}\|^2 + (J(\boldsymbol{\sigma}\circ\boldsymbol{\xi})\mathbf{F}^{-T}, \nabla\mathbf{v}) + (J(\nabla\mathbf{v}_1\mathbf{F}^{-1}\mathbf{v}),\mathbf{v}) \\ = \left(J\left[\mathbf{f} - \frac{\partial\mathbf{v}_1}{\partial t} - (\nabla\mathbf{v}_1)\mathbf{F}^{-1}(\mathbf{v}_1-\boldsymbol{\xi}_t)\right],\mathbf{v}\right).\end{aligned}$$

Using the notation $\mathbf{D}_\xi(\mathbf{v}) = \frac{1}{2}(\nabla\mathbf{v}\mathbf{F}^{-1} + \mathbf{F}^{-T}(\nabla\mathbf{v})^T)$ for the rate of deformation tensor in the reference coordinates, we get with the help of (8) and the second equation in (4)

$$\begin{aligned}(J(\boldsymbol{\sigma}\circ\boldsymbol{\xi})\mathbf{F}^{-T}, \nabla\mathbf{v}) &= (J(-p\mathbf{I} + \nu(\nabla\mathbf{u}\mathbf{F}^{-1} + \mathbf{F}^{-T}(\nabla\mathbf{u})^T))\mathbf{F}^{-T}, \nabla\mathbf{v}) = 2\nu(J\mathbf{D}_\xi(\mathbf{u})\mathbf{F}^{-T}, \nabla\mathbf{v}) \\ &= 2\nu(J\mathbf{D}_\xi(\mathbf{u}), \nabla\mathbf{v}\mathbf{F}^{-1}) = 2\nu(J\mathbf{D}_\xi(\mathbf{u}), \mathbf{D}_\xi(\mathbf{v})).\end{aligned}$$

In the last equality we used that for any symmetric tensor $\mathbf{A}$ and any tensor $\mathbf{B}$, it holds $\mathbf{A} : \mathbf{B} = \frac{1}{2}\mathbf{A} : (\mathbf{B} + \mathbf{B}^T)$. Hence, using the splitting $\mathbf{u} = \mathbf{v} + \mathbf{v}_1$ we get

$$(J(\boldsymbol{\sigma}\circ\boldsymbol{\xi})\mathbf{F}^{-T}, \nabla\mathbf{v}) = 2\nu\|J^{\frac{1}{2}}\mathbf{D}_\xi(\mathbf{v})\|^2 + 2\nu(\operatorname{div}(J\mathbf{D}_\xi(\mathbf{v}_1)\mathbf{F}^{-T}),\mathbf{v}).$$

Therefore, the energy balance equality in ALE coordinates takes the form

$$\frac{1}{2}\frac{d}{dt}\|J^{\frac{1}{2}}\mathbf{v}\|^2 + 2\nu\|J^{\frac{1}{2}}\mathbf{D}_\xi(\mathbf{v})\|^2 + (J(\nabla\mathbf{v}_1\mathbf{F}^{-1}\mathbf{v}),\mathbf{v}) = (\widetilde{\mathbf{f}},\mathbf{v}), \tag{11}$$

where $\widetilde{\mathbf{f}} = \left(J(\mathbf{f} - \frac{\partial\mathbf{v}_1}{\partial t} - (\nabla\mathbf{v}_1)\mathbf{F}^{-1}(\mathbf{v}_1-\boldsymbol{\xi}_t)) + 2\nu\operatorname{div}(J\mathbf{D}_\xi(\mathbf{v}_1)\mathbf{F}^{-T})\right) \in L^2(0,T;H^{-1}(\Omega_0))$ accounts for all external forces, including volume forces and those exerted on the fluid by the evolving boundary. The mechanical interpretation of (11) is the following one: the work of all external forces (right-hand side) is balanced by the change of kinetic energy (the first term), energy of viscous dissipation (the second term), and flow intensification due to the boundary condition (the third term).

2.2 Weak formulation

We need some preliminaries. We start with Korn's-type inequality in the reference domain,

$$\|\nabla \mathbf{u}\| \le C_K \|J^{\frac{1}{2}} \mathbf{D}_\xi(\mathbf{u})\| \quad \forall\ \mathbf{u} \in H_0^1(\Omega_0)^d, \quad t \in [0,T], \tag{12}$$

with C_K uniformly bounded with respect to $t \in [0,T]$. To show (12), one uses assumptions (1) and Korn's inequality for functions vanishing on the boundary: For any $t \in [0,T]$, we have

$$\begin{aligned}
\|\nabla \mathbf{u}\| &= \|J^{-\frac{1}{2}} \nabla(\mathbf{u} \circ \boldsymbol{\xi}^{-1})\mathbf{F}\|_{L^2(\Omega(t))} \le C_F c_J^{-\frac{1}{2}} \|\nabla(\mathbf{u} \circ \boldsymbol{\xi}^{-1})\|_{L^2(\Omega(t))} \\
&= \frac{1}{\sqrt{2}} C_F c_J^{-\frac{1}{2}} \|\nabla(\mathbf{u} \circ \boldsymbol{\xi}^{-1}) + \nabla^T(\mathbf{u} \circ \boldsymbol{\xi}^{-1})\|_{L^2(\Omega(t))} \\
&= \sqrt{2} C_F c_J^{-\frac{1}{2}} \|J^{\frac{1}{2}} \mathbf{D}_\xi(\mathbf{u})\|.
\end{aligned}$$

For $t \in [0,T]$ we now introduce the following time-dependent trilinear and bilinear forms:

$$\begin{aligned}
c(\boldsymbol{\xi}; \mathbf{w}, \mathbf{u}, \boldsymbol{\psi}) &= \int_{\Omega_0} J \left((\nabla \mathbf{u}) \mathbf{F}^{-1} \mathbf{w} \right) \cdot \boldsymbol{\psi} \, \mathrm{d}\mathbf{x}, \quad \mathbf{w}, \mathbf{u}, \boldsymbol{\psi} \in H^1(\Omega_0)^d, \\
a(\boldsymbol{\xi}; \mathbf{u}, \boldsymbol{\psi}) &= \int_{\Omega_0} 2\nu J \mathbf{D}\mathbf{u} : \mathbf{D}\boldsymbol{\psi} \, \mathrm{d}\mathbf{x}, \quad \mathbf{u}, \boldsymbol{\psi} \in H^1(\Omega_0)^d, \\
b(\boldsymbol{\xi}; p, \boldsymbol{\psi}) &= \int_{\Omega_0} p J \mathbf{F}^{-T} : \nabla \boldsymbol{\psi} \, \mathrm{d}\mathbf{x}, \quad p \in L^2(\Omega_0),\ \boldsymbol{\psi} \in H^1(\Omega_0)^d.
\end{aligned}$$

Thanks to (1) and the Korn's-type inequality (12) the bilinear form $a(\boldsymbol{\xi}(t); \cdot, \cdot)$ is coercive and continuous on $H_0^1(\Omega_0)^d \times H_0^1(\Omega_0)^d$ uniformly in time and $b(\boldsymbol{\xi}(t); \cdot, \cdot)$ is continuous on $L^2(\Omega_0) \times H_0^1(\Omega_0)^d$ uniformly in time. The weak formulation of (4) reads: Find $\{\mathbf{v}, p\} \in L^2(0,T; H_0^1(\Omega_0)^d) \cap L^\infty(0,T; L^2(\Omega_0)^d) \times L^2(Q)$ satisfying

$$\begin{aligned}
(J\mathbf{v}_t, \boldsymbol{\psi}) + c(\boldsymbol{\xi}; \mathbf{u} - \boldsymbol{\xi}_t, \mathbf{v}, \boldsymbol{\psi}) + c(\boldsymbol{\xi}; \mathbf{v}, \mathbf{v}_1, \boldsymbol{\psi}) + a(\boldsymbol{\xi}; \mathbf{v}, \boldsymbol{\psi}) \\
- b(\boldsymbol{\xi}; p, \boldsymbol{\psi}) + b(\boldsymbol{\xi}; q, \mathbf{v}) = (\widetilde{\mathbf{f}}, \boldsymbol{\psi})
\end{aligned} \tag{13}$$

for all $\boldsymbol{\psi} \in H_0^1(\Omega_0)^d$, $q \in L^2(\Omega_0)$ for all $t \in [0,T]$ in the sense of distribution.

3 Discretization method

In this section we introduce both time and space discretizations of the formulation (4) in the reference domain. Treating the problem in reference coordinates allows us to avoid triangulations and finite element function spaces dependent on time. In this paper, we assume that the mapping $\boldsymbol{\xi}$ and velocity $\mathbf{v}_1$ are given explicitly and are used in the finite element formulation without any further numerical approximation.

Let a collection of simplices $\mathcal{T}_h$ (triangles in $d = 2$ and tetrahedra in $d = 3$) form a consistent regular triangulation $\mathcal{T}_h$ of the reference domain $\overline{\Omega}_0$. Consider conforming FE spaces $\mathbb{V}_h \subset H^1(\Omega_0)^d$ and $\mathbb{Q}_h \subset L^2(\Omega_0)$; $\mathbb{V}_h^0$ is a subspace of $\mathbb{V}_h$ of functions vanishing on the boundary of $\mathcal{T}_h$. We assume that $\mathbb{V}_h^0$ and $\mathbb{Q}_h$ form the LBB-stable finite element pair: There exists a mesh-independent constant c_0, such that

$$\inf_{q_h \in \mathbb{Q}_h} \sup_{\mathbf{v}_h \in \mathbb{V}_h^0} \frac{(q_h, \operatorname{div} \mathbf{v}_h)}{\|\nabla \mathbf{v}_h\| \|q_h\|} \ge c_0 > 0. \tag{14}$$

As an example of admissible discretization, we consider the generalized Taylor-Hood finite element spaces,

$$\begin{aligned} \mathbb{V}_h &= \{\mathbf{u}_h \in C(\Omega_0)^d \,:\, \mathbf{u}_h|_T \in \left[P^{m+1}(T)\right]^d, \forall\, T \in \mathcal{T}_h\}, \\ \mathbb{Q}_h &= \{q_h \in C(\Omega_0) \,:\, q_h|_T \in P^m(T), \forall\, T \in \mathcal{T}_h\}, \end{aligned} \tag{15}$$

where integer $m \geq 1$ is a polynomial degree.

Assuming a constant time step $\Delta t = \frac{T}{N}$, we use the notation $\mathbf{v}^k(\mathbf{x}) := \mathbf{v}(k\Delta t, \mathbf{x})$, and similar for p and $\boldsymbol{\xi}$. To emphasize the dependence on k, denote $\mathbf{F}_k := \nabla \boldsymbol{\xi}^k$, $J_k := \det(\mathbf{F}(\boldsymbol{\xi}^k))$, $\mathbf{D}_k(\mathbf{v}) := \mathbf{D}_{\xi^k}(\mathbf{v})$.

For given spatial functions f^i, $i = 0, \ldots, k$, $[f]_t^k := \frac{f^k - f^{k-1}}{\Delta t}$ denotes the backward finite difference at $t = k\Delta t$. Let $\mathbf{v}_h^0$ be the Lagrange interpolant of the initial velocity field. The linearized finite element discretization of (13) reads: For $k = 1, 2, \ldots$, find $\{\mathbf{v}_h^k, p_h^k\} \in \mathbb{V}_h^0 \times \mathbb{Q}_h$ satisfying for all $\boldsymbol{\psi}_h \in \mathbb{V}_h^0$, $q_h \in \mathbb{Q}_h$

$$\begin{aligned} \left(J_{k-1}\,[\mathbf{v}_h]_t^k\,, \boldsymbol{\psi}_h\right) + \left(\frac{1}{2}\,[J]_t^k\,\mathbf{v}_h^k, \boldsymbol{\psi}_h\right) + \frac{1}{2}(\mathrm{div}\,\left(J_k \mathbf{F}_k^{-1}\mathbf{w}_h^k\right)\mathbf{v}_h^k, \boldsymbol{\psi}_h) \\ + c(\boldsymbol{\xi}^k; \mathbf{w}_h^k, \mathbf{v}_h^k, \boldsymbol{\psi}_h) + c(\boldsymbol{\xi}^k; \mathbf{v}_h^k, \mathbf{v}_1^k, \boldsymbol{\psi}_h) + a(\boldsymbol{\xi}^k; \mathbf{v}_h^k, \boldsymbol{\psi}_h) \\ - b(\boldsymbol{\xi}^k; p_h^k, \boldsymbol{\psi}_h) + b(\boldsymbol{\xi}^k; q_h, \mathbf{v}_h^k) = (\widetilde{\mathbf{f}}^k, \boldsymbol{\psi}_h) \end{aligned} \tag{16}$$

with ALE advection velocity $\mathbf{w}_h^k := \left(\mathbf{v}_h^{k-1} + \mathbf{v}_1^{k-1} - [\boldsymbol{\xi}]_t^{k-1}\right)$.

The second and the third terms in (16) are consistent due to the identity (7) and are added in the FE formulation to enforce the conservation property of the discretization. While our computations show that in practice this term can be skipped, we need these terms for the stability bound in the next section. In the numerical analysis of incompressible Navier-Stokes equations in the Eulerian description, including these terms corresponds to the Temam's skew-symmetric form of the convective terms [22].

Note that the inertia terms are linearized so that a *linear* algebraic system should be solved on each time step. In the next section we show that the finite element method is energy stable.

4 Stability of FEM solution

First we test (16) with $\boldsymbol{\psi}_h = \mathbf{v}_h^k$, $q_h = p_h^k$. We handle each resulting term separately and start with the first term in (16):

$$\begin{aligned} (J_{k-1}\,[\mathbf{v}_h]_t^k\,, \mathbf{v}_h^k) = \frac{1}{2\Delta t}\left(\|J_k^{\frac{1}{2}}\mathbf{v}_h^k\|^2 - \|J_{k-1}^{\frac{1}{2}}\mathbf{v}_h^{k-1}\|^2\right) \\ - \frac{1}{2}([J]_t^k\,\mathbf{v}_h^k, \mathbf{v}_h^k) + \frac{\Delta t}{2}\|J_{k-1}^{\frac{1}{2}}\,[\mathbf{v}_h]_t^k\,\|^2\,. \end{aligned} \tag{17}$$

Applying (10) to the fourth (inertia) term in (16) and using boundary conditions give

$$(J_k(\nabla \mathbf{v}_h^k \mathbf{F}_k^{-1}\mathbf{w}_h^k), \mathbf{v}_h^k) = -\frac{1}{2}(\mathrm{div}\,\left(J_k \mathbf{F}_k^{-1}\mathbf{w}_h^k\right)\mathbf{v}_h^k, \mathbf{v}_h^k). \tag{18}$$

The sixth term in (16) gives

$$a(\boldsymbol{\xi}^k; \mathbf{v}_h^k, \mathbf{v}_h^k) = 2\nu\left(J_k \mathbf{D}_k(\mathbf{v}_h^k), \mathbf{D}_k(\mathbf{v}_h^k)\right) = 2\nu\left\|J_k^{\frac{1}{2}}\mathbf{D}_k(\mathbf{v}_h^k)\right\|^2.$$

The b-terms cancel out for $q_h = p_h^k$. Substituting all equalities back into (16), we obtain after some cancellations the following energy balance for the finite element problem:

$$\underbrace{\frac{1}{2\Delta t}\left(\|J_k^{\frac{1}{2}}\mathbf{v}_h^k\|^2 - \|J_{k-1}^{\frac{1}{2}}\mathbf{v}_h^{k-1}\|^2\right)}_{\substack{\text{variation of}\\ \text{kinetic energy}}} \underbrace{+2\nu\left\|J_k^{\frac{1}{2}}\mathbf{D}_k(\mathbf{v}_h^k)\right\|^2}_{\substack{\text{energy of}\\ \text{viscous dissipation}}} \underbrace{+\frac{(\Delta t)}{2}\left\|J_{k-1}^{\frac{1}{2}}[\mathbf{v}_h]_t^k\right\|^2}_{\substack{O(\Delta t)\text{ dissipative}\\ \text{term}}} \underbrace{+(J_k(\nabla\mathbf{v}_1^k\mathbf{F}_k^{-1})\mathbf{v}_h^k,\mathbf{v}_h^k)}_{\substack{\text{intensification}\\ \text{due to b.c.}}}$$
$$= \underbrace{(\widetilde{\mathbf{f}}^k,\mathbf{v}_h^k)}_{\substack{\text{work of}\\ \text{ext. forces}}} \tag{19}$$

One notes that the above equality resembles the energy balance (11) of the original flow problem up to a $O(\Delta t)$ term. The $O(\Delta t)$ term in (19) is non-negative and dropping it changes the equality to inequality. We deduce an energy stability estimate for the finite element method from the balance in (19). To this end, we introduce $\|\cdot\|_k := \left(\int_{\Omega_0} J_k|\cdot|^2\,\mathrm{d}\mathbf{x}\right)^{\frac{1}{2}}$, which defines a k-dependent norm uniformly equivalent to the L^2-norm.

Thanks to Sobolev's embedding inequalities as well as (1) and (12), we bound the intensification term resulting from the boundary motion in two ways,

$$|(J_k(\nabla\mathbf{v}_1^k\mathbf{F}_k^{-1})\mathbf{v}_h^k,\mathbf{v}_h^k)| \le \begin{cases} C\|\nabla\mathbf{v}_1^k\|\|\nabla\mathbf{v}_h^k\|^2 \le C_1\|\nabla\mathbf{v}_1^k\|\|\mathbf{D}_k(\mathbf{v}_h^k)\|_k^2, \\ C\|\nabla\mathbf{v}_1^k\|_{L^\infty(\Omega_0)}\|\mathbf{v}_h^k\|^2 \le C_2\|\mathbf{v}_h^k\|_k^2. \end{cases}$$

If the factor $C_1\|\nabla\mathbf{v}_1^k\|$ is not too large so that it holds

$$C_1\|\nabla\mathbf{v}_1^k\| \le \nu/2, \tag{20}$$

then the intensification term can be absorbed by the viscous dissipation term. We handle the forcing term in a standard way with the help of the Cauchy and the Korn inequality (12). So we obtain from (19)

$$\frac{1}{2}\|\mathbf{v}_h^k\|_k^2 + \nu\Delta t\|\mathbf{D}_k(\mathbf{v}_h^k)\|_k^2 \le \frac{1}{2}\|\mathbf{v}_h^{k-1}\|_{k-1}^2 + C\Delta t\|\widetilde{\mathbf{f}}^k\|^2. \tag{21}$$

Summing up inequalities (21) for $k = 1,\dots,n$, $n \le N$, gives

$$\frac{1}{2}\|\mathbf{v}_h^n\|_n^2 + \nu\sum_{k=1}^n \Delta t\|\mathbf{D}_k(\mathbf{v}_h^k)\|_k^2 \le \frac{1}{2}\|\mathbf{v}_0\|_0^2 + C\sum_{k=1}^n \Delta t\|\widetilde{\mathbf{f}}^k\|^2. \tag{22}$$

Otherwise, if (20) does not hold, we estimate

$$\frac{1}{2}(1-2C_2\Delta t)\|\mathbf{v}_h^k\|_k^2 + \nu\Delta t\|\mathbf{D}_k(\mathbf{v}_h^k)\|_k^2 \le \frac{1}{2}\|\mathbf{v}_h^{k-1}\|_{k-1}^2 + C\Delta t\|\widetilde{\mathbf{f}}^k\|^2. \tag{23}$$

Now we assume that Δt is sufficiently small such that $(1-2C_2\Delta t) = \alpha > 0$. Summing over $k = 1,\dots,n$, gives

$$\frac{1}{2}\|\mathbf{v}_h^n\|_n^2 + \nu\sum_{k=1}^n \Delta t\|\mathbf{D}_k(\mathbf{v}_h^k)\|_k^2 \le C_2\sum_{k=1}^n \Delta t\|\mathbf{v}_h^k\|_k^2 + \frac{1}{2}\|\mathbf{v}_0\|_0^2 + C\sum_{k=1}^n \Delta t\|\widetilde{\mathbf{f}}^k\|^2. \tag{24}$$

With the help of the discrete Gronwall lemma, e.g. [23], inequality (24) yields

$$\frac{1}{2}\|\mathbf{v}_h^n\|_n^2 + \nu\sum_{k=1}^{n}\Delta t\|\mathbf{D}_k(\mathbf{v}_h^k)\|_k^2 \le e^{\frac{2C_2}{\alpha}T}\left(\frac{1}{2}\|\mathbf{v}_0\|_0^2 + C\sum_{k=1}^{n}\Delta t\|\widetilde{\mathbf{f}}^k\|^2\right). \tag{25}$$

Estimates (22) and (25) show the energy stability of the finite element method. The first of these two inequalities holds if (20) is satisfied.

5 Application to the left ventricle hemodynamics

We illustrate the performance of our method for solving the Navier-Stokes equations in a moving domain. The method is applied to simulate a flow in a model of the left ventricle of a human heart. The hemodynamics of the heart is characterized by transitional or even turbulent blood flows, see e.g. [6, 24, 25]. Therefore, realistic simulations should employ a subgrid model, such as Large Eddy Simulation (LES) model of turbulence [6], unless the mesh is sufficiently fine to resolve all scales in the flow. The choice and calibration of a suitable turbulence model is beyond the scope of this study. To be able to compute stable solutions with the FE method (16) on a realistic mesh, we consider a larger blood viscosity: we set $\nu = 4 \cdot 10^{-5}\ m^2/s$; it is about 10 times larger than the true viscosity. For the same reason we smooth in time the motion of the heart wall during the diastole phase, see details below. We consider the left ventricle due to its hemodynamic significance, but the method is equally applicable to the right ventricle.

The motion of the ventricle is recovered from a sequence of ceCT images of a real patient. The recovered data provides displacement field for the ventricle's wall, which is used in the FE method (16). The input data was a dataset of 100 images with $512 \times 512 \times 480$ voxels and $0.625 \times 0.625 \times 0.25$ mm resolution. The images were taken from a chest ceCT of a 50-years-old female.

First we build a dynamic grid model. Next we use this auxiliary dynamic grid to define the mapping $\boldsymbol{\xi}$ in our quasi-Lagrangian method. We recall that all computations in our FE method are done on a fixed reference mesh. The dynamic grid model is built in several steps. At the first stage, the images are preprocessed by the 3D non-local means smoothing [26], and then cropped down and resampled to the region of interest. For the machine-learning stage of the reconstruction, we select three images at different stages of cardiac cycle: the beginning of systole, the end of systole, and the middle of rapid inflow during diastole. We perform a manual segmentation of these three images using the level set method from ITK-SNAP package [27]. Next, all the remaining images are segmented by the machine learning technique with the random forest classifier [28], which was trained on the manually segmented images. At the next stage, the segmentation is smoothed, and its subsequent correction is performed with the help of mathematical operations such as dilation, erosion, and construction of connected regions. The valve areas are identified in each image as the interface between the ventricle and the atrium and the interface between the ventricle and the aorta. We average the valve areas over all the images to determine the unique position of the valve planes. To simplify the mesh generation and numerical modeling, the valve planes are assumed to be intact during the cardiac cycle.

Application of the Delaunay triangulation from CGAL Mesh library [29] for the first segmented image yields an unstructured tetrahedral mesh with typical mesh size of 0.7 mm. Within the mesh, the left ventricle is defined implicitly by segmented image, the valve planes are defined explicitly. We enforce each tetrahedron to have at least one internal node by splitting each cell with four boundary nodes. The main requirement for a 3D dynamic grid model

of the heart ventricle is to preserve mesh connectivity: in the sequence of grids only nodal positions change. We deform the mesh by node movements for each subsequent image. At the first stage, we move only boundary nodes while simultaneously propagating and smoothing the surface mesh. Each boundary node is shifted in the direction of the weighted sum of two vectors: the surface normal vector (weight 0.2) and the vector pointing at the center of surrounding nodes (weight 0.4). This procedure is repeated until the maximum displacement drops below $\varepsilon = 0.001$ mm, or until the maximum number of 2000 iterations is exceeded. Note that the above algorithm does not recover the material trajectories of ventricle points and therefore may produce spurious tangential velocities on the boundary, see Remark 1. We pay special attention to the nodes on the valve planes: they should always stay on the planes (Fig. 1). At the second stage, we apply simultaneous untangling and smoothing algorithm [30]; the boundary nodes are fixed, and only the internal nodes are shifted. The untangling stage is robust due to the presence of internal nodes in all tetrahedra. The final output is the series of *topologically invariant* meshes with 14033 nodes, 88150 edges and 69257 tetrahedra for the left ventricle recovered from the dynamic ceCT images (Fig. 2).

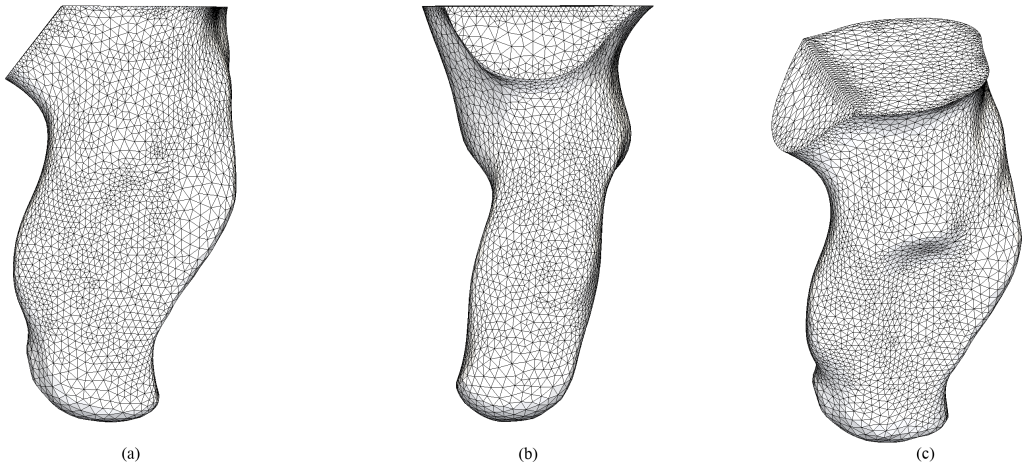

Figure 1: The ventricle surface mesh at the end of systole, $t = 300$ ms: (a) horizontal long axis view, (b) vertical long axis view, (c) anterior view.

To set up the boundary conditions, we split the left ventricle boundary into several patches shown in Fig. 3. All the patches are time-dependent, but the flat patches labeled as 2 through 5 do not leave their planes during the motion. We assume that the blood leaves the ventricle through the aortic valve 2 during the systole phase, while the mitral valve 5 is connected to the atrium and sucks blood in during the expansion stage called diastole. Patches 3 and 4 lie in the same planes as patches 2 and 5, respectively. Both of these sites are not involved in the blood transfer and serve as separators between the valves.

At the initial moment of time, the beginning of the systole stage, we assume the system is at rest with zero pressure.

The impact of the valves is taken into account in the model through appropriate boundary conditions. The ventricle passes through the systole phase approximately until $t = 355$ ms releasing blood flow through the aortic valve. During this time interval, we set the "do-nothing" boundary condition (3) with $\hat{\mathbf{g}} = \mathbf{0}$ on the patch with label 2. For the remaining time interval ending at $T = 1.2573$ s, we impose the analogous condition on the patch with label 5. Finally, on all other sites, including valve 2 during the diastole phase and valve 5 during the systole phase, the no-penetration no-slip condition (2) is imposed, $\mathbf{u} = \boldsymbol{\xi}_t$.

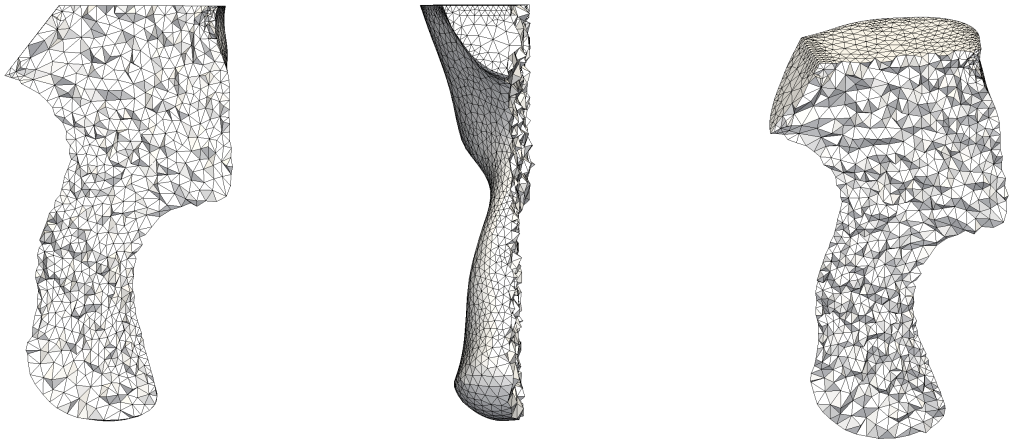

Figure 2: Section of the volumetric mesh at the end of systole, $t = 300$ ms: (a) horizontal long axis view, (b) vertical long axis view, (c) anterior view.

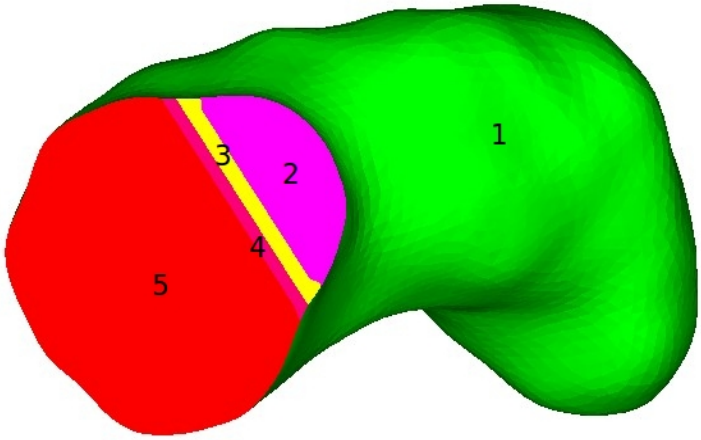

Figure 3: Left ventricle with marked surface labels: wall surface 1, aortic valve 2, mitral valve 5, separators 3 and 4.

We note that both "do-nothing" and no-penetration no-slip conditions on valve sites are simplifications. We plan to implement more realistic generalizations [31] in a future.

The reference domain Ω_0 is given by the mesh at time $t = 0$. For the spatial discretization of the equations in Ω_0, we use the minimal degree Taylor-Hood finite element spaces (15) with $m = 1$. This leads to linear systems with 320582 unknowns, comprised of 14033 nodal pressure degrees of freedom and 14033+88150 degrees of freedom residing at the mesh vertices and edge centers, for each velocity component. Denote by $\mathbf{x}$ the spatial coordinates of a node of the reference grid at time $t = 0$, and identify the coordinates $\boldsymbol{\xi}(\mathbf{x}, t)$ of the corresponding node at time $t = t^k$. We now define the mapping $\boldsymbol{\xi}^k$ as the continuous piecewise linear vector function on the reference grid, which takes the values $\boldsymbol{\xi}(\mathbf{x}, t)$ at the reference grid nodes $\mathbf{x}$.

Omitting the second and the third terms in (16) (see the comment right after (16)), we can rewrite the method in the following convenient form: Find velocity $\mathbf{u}^k \in \mathbb{V}_h$ and pressure $p^k \in \mathbb{Q}_h$ satisfying equation

$$\begin{aligned}
&\int_{\Omega_0} J_k \frac{\mathbf{u}^k - \mathbf{u}^{k-1}}{\Delta t} \cdot \boldsymbol{\psi} \, \mathrm{d}\mathbf{x} + + \int_{\Omega_0} J_k \nabla \mathbf{u}^k \mathbf{F}_k^{-1} \left(\mathbf{u}^{k-1} - \frac{\boldsymbol{\xi}^k - \boldsymbol{\xi}^{k-1}}{\Delta t} \right) \cdot \boldsymbol{\psi} \, \mathrm{d}\mathbf{x} \\
&- \int_{\Omega_0} J_k p^k \mathbf{F}_k^{-T} : \nabla \boldsymbol{\psi} \, \mathrm{d}\mathbf{x} + \int_{\Omega_0} J_k q \mathbf{F}_k^{-T} : \nabla \mathbf{u}^k \, \mathrm{d}\mathbf{x} \\
&+ \int_{\Omega_0} \nu J_k (\nabla \mathbf{u}^k \mathbf{F}_k^{-1} \mathbf{F}_k^{-T} + \mathbf{F}_k^{-T} (\nabla \mathbf{u}^k)^T \mathbf{F}_k^{-T}) : \nabla \boldsymbol{\psi} \, \mathrm{d}\mathbf{x} = 0
\end{aligned} \tag{26}$$

and the no-penetration no-slip $\mathbf{u}^k = (\boldsymbol{\xi}^k - \boldsymbol{\xi}^{k-1})/\Delta t$ or the "do-nothing" boundary conditions, for all $\boldsymbol{\psi}$ and q from the appropriate FE spaces.

We note that the time between two adjacent frames (and meshes) is equal to 12.7 milliseconds. Given the fast motion of the ventricle, such time step turned out to be too large to deliver acceptable accuracy. Therefore, we take a step 20 times smaller, i.e. $\Delta t = 0.635$ ms, and generate a new series of meshes in the pre-processing phase. The intermediate meshes are interpolated by cubic splines from the available 100 meshes. The enriched mesh sequence contains 1981 meshes instead of 100. The calculation does not reveal any time instance at which the condition $J > 0$ is violated. This indicates a good quality of the resulting series of meshes.

In order to reduce the observed ventricle volume rate causing extremely high influx velocities at the diastole phase, we constructed five new mesh sets by applying a different level of time smoothing for the wall displacements. Fig. 4 shows the dependence of the ventricle volume on time for all of these meshes. The volume curves, starting from the closest to the original one, are marked as A, B, C, D, E. The simulation of the entire cardiac cycle was successful for the mesh sequences C, D, and E.

The velocity streamlines and the Q-criterion at 300 ms (the systole phase) are shown in Fig. 5 and Fig. 6, respectively.

6 Conclusion

We presented a finite element method for the solution of the Navier-Stokes equations in a time-dependent domain. The method requires the solution of a linear system on each time step. The stability estimate does not require a CFL time-step restriction.

We demonstrated applicability of the method by simulating a flow in the human left ventricle. The moving mesh sequence was generated from anonymized ceCT images. The shortcoming of the ceCT modality is lack of information about the tangential velocity of the ventricle

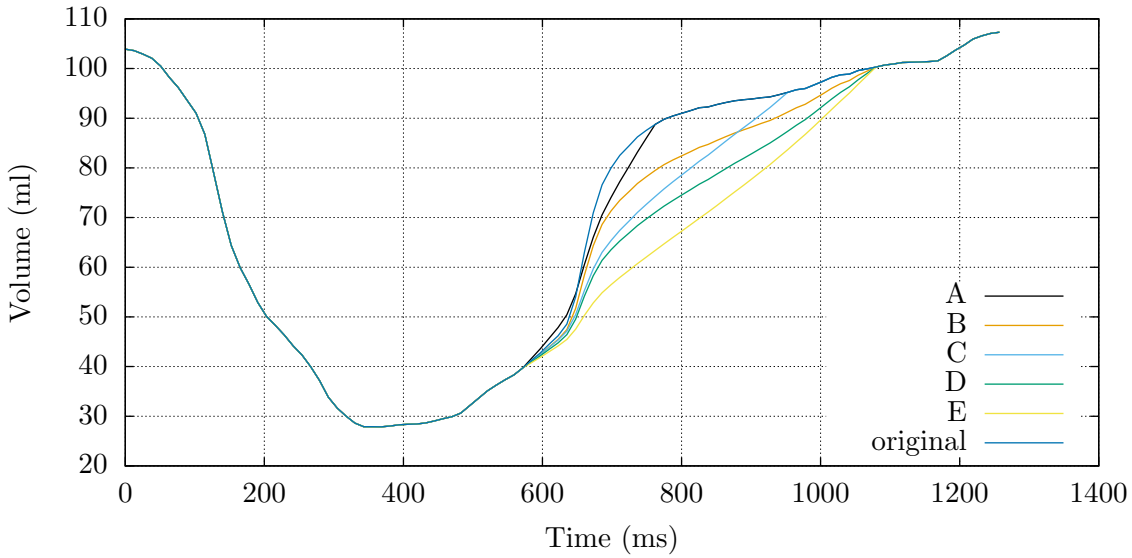

Figure 4: The ventricle volume change in time for six different domains, including the original one

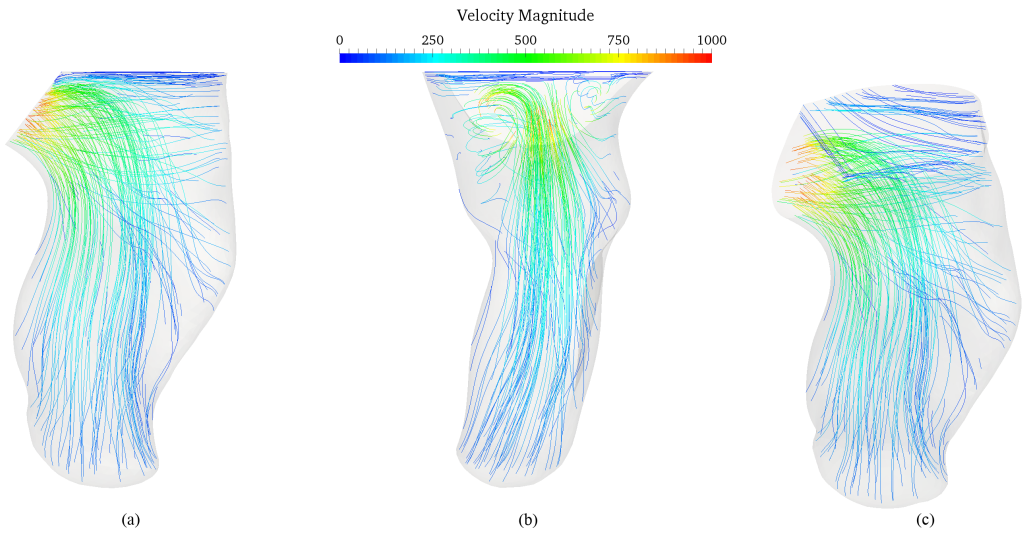

Figure 5: Velocity streamlines at the end of systole, $t = 300$ ms: (a) horizontal long axis view, (b) vertical long axis view, (c) anterior view.

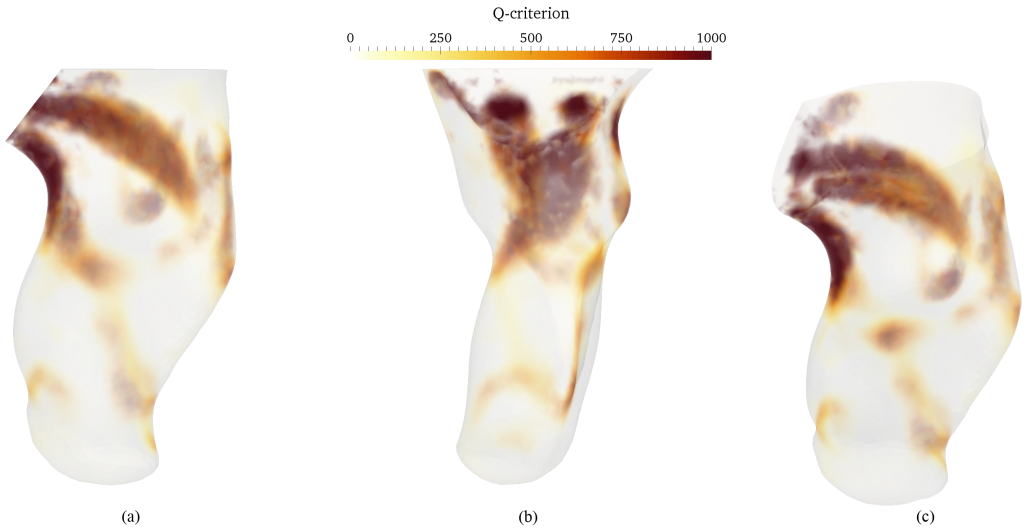

Figure 6: Q-criterion at the end of systole, $t = 300$ ms: (a) horizontal long axis view, (b) vertical long axis view, (c) anterior view.

wall. A possible solution is the use of the 4D Ultra Sound image dataset. Our forthcoming paper addresses error analysis of the finite element method (16). In a future we plan to add a subgrid model to be able to compute realistic hemodynamics of the heart.

References

[1] N. R. Saber, N. B. Wood, A. Gosman, R. D. Merrifield, G.-Z. Yang, C. L. Charrier, P. D. Gatehouse, D. N. Firmin, Progress towards patient-specific computational flow modeling of the left heart via combination of magnetic resonance imaging with computational fluid dynamics, Annals of biomedical engineering 31 (1) (2003) 42–52.

[2] Q. Long, R. Merrifield, X. Xu, P. Kilner, D. Firmin, G. Yang, Subject-specific computational simulation of left ventricular flow based on magnetic resonance imaging, Proceedings of the Institution of Mechanical Engineers, Part H: Journal of Engineering in Medicine 222 (4) (2008) 475–485.

[3] T. Schenkel, M. Malve, M. Reik, M. Markl, B. Jung, H. Oertel, MRI-based CFD analysis of flow in a human left ventricle: methodology and application to a healthy heart, Annals of biomedical engineering 37 (3) (2009) 503–515.

[4] V. Mihalef, R. I. Ionasec, P. Sharma, B. Georgescu, I. Voigt, M. Suehling, D. Comaniciu, Patient-specific modelling of whole heart anatomy, dynamics and haemodynamics from four-dimensional cardiac ct images, Interface Focus 1 (3) (2011) 286–296.

[5] T. Doenst, K. Spiegel, M. Reik, M. Markl, J. Hennig, S. Nitzsche, F. Beyersdorf, H. Oertel, Fluid-dynamic modeling of the human left ventricle: methodology and application to surgical ventricular reconstruction, The Annals of thoracic surgery 87 (4) (2009) 1187–1195.

[6] C. Chnafa, S. Mendez, F. Nicoud, Image-based large-eddy simulation in a realistic left heart, Computers & Fluids 94 (2014) 173–187.

[7] R. Mittal, J. H. Seo, V. Vedula, Y. J. Choi, H. Liu, H. H. Huang, S. Jain, L. Younes, T. Abraham, R. T. George, Computational modeling of cardiac hemodynamics: current status and future outlook, Journal of Computational Physics 305 (2016) 1065–1082.

[8] B. Su, R. San Tan, J. Le Tan, K. W. Q. Guo, J. M. Zhang, S. Leng, X. Zhao, J. C. Allen, L. Zhong, Cardiac MRI based numerical modeling of left ventricular fluid dynamics with mitral valve incorporated, Journal of biomechanics 49 (7) (2016) 1199–1205.

[9] A. Masud, T. J. Hughes, A space-time Galerkin/least-squares finite element formulation of the Navier-Stokes equations for moving domain problems, Computer Methods in Applied Mechanics and Engineering 146 (1-2) (1997) 91–126.

[10] T. E. Tezduyar, M. Behr, S. Mittal, J. Liou, A new strategy for finite element computations involving moving boundaries and interfacesthe deforming-spatial-domain/space-time procedure: II. computation of free-surface flows, two-liquid flows, and flows with drifting cylinders, Computer methods in applied mechanics and engineering 94 (3) (1992) 353–371.

[11] S. Osher, R. Fedkiw, Level set methods and dynamic implicit surfaces, Vol. 153, Springer Science & Business Media, 2006.

[12] R. Glowinski, T.-W. Pan, T. I. Hesla, D. D. Joseph, A distributed Lagrange multiplier/fictitious domain method for particulate flows, International Journal of Multiphase Flow 25 (5) (1999) 755–794.

[13] C. S. Peskin, Numerical analysis of blood flow in the heart, Journal of computational physics 25 (3) (1977) 220–252.

[14] S. Groß, A. Reusken, An extended pressure finite element space for two-phase incompressible flows with surface tension, Journal of Computational Physics 224 (1) (2007) 40–58.

[15] C. Hirt, A. A. Amsden, J. Cook, An arbitrary Lagrangian-Eulerian computing method for all flow speeds, Journal of computational physics 14 (3) (1974) 227–253.

[16] F. Nobile, L. Formaggia, A stability analysis for the arbitrary lagrangian: Eulerian formulation with finite elements, East-West Journal of Numerical Mathematics 7 (EPFL-ARTICLE-176278) (1999) 105–132.

[17] F. Duarte, R. Gormaz, S. Natesan, Arbitrary Lagrangian–Eulerian method for Navier–Stokes equations with moving boundaries, Computer Methods in Applied Mechanics and Engineering 193 (45) (2004) 4819–4836.

[18] R. Guberovic, C. Schwab, R. Stevenson, Space-time variational saddle point formulations of Stokes and Navier–Stokes equations, ESAIM: Mathematical Modelling and Numerical Analysis 48 (3) (2014) 875–894.

[19] J. Sudirham, J. Van Der Vegt, R. Van Damme, Space–time discontinuous Galerkin method for advection–diffusion problems on time-dependent domains, Applied numerical mathematics 56 (12) (2006) 1491–1518.

[20] J. Martin, L. Smaranda, T. Takahashi, Convergence of a finite element/ALE method for the Stokes equations in a domain depending on time, Journal of Computational and Applied Mathematics 230 (2009) 521–545.

[21] T. Miyakawa, Y. Teramoto, Existence and periodicity of weak solutions of the Navier-Stokes equations in a time dependent domain, Hiroshima Mathematical Journal 12 (3) (1982) 513–528.

[22] R. Temam, Navier-Stokes equations: theory and numerical analysis, Vol. 343, American Mathematical Soc., 2001.

[23] W. Layton, Introduction to the numerical analysis of incompressible viscous flows, Vol. 6, Siam, 2008.

[24] G. Querzoli, S. Fortini, A. Cenedese, Effect of the prosthetic mitral valve on vortex dynamics and turbulence of the left ventricular flow, Physics of fluids 22 (4) (2010) 041901.

[25] A. Falahatpisheh, A. Kheradvar, High-speed particle image velocimetry to assess cardiac fluid dynamics in vitro: from performance to validation, European Journal of Mechanics-B/Fluids 35 (2012) 2–8.

[26] A. Buades, B. Coll, J. M. Morel, A review of image denoising algorithms, with a new one, Multiscale Modeling & Simulation 4 (2) (2005) 490–530.

[27] P. A. Yushkevich, J. Piven, H. C. Hazlett, R. G. Smith, S. Ho, J. C. Gee, G. Gerig, User-guided 3D active contour segmentation of anatomical structures: Significantly improved efficiency and reliability, NeuroImage 31 (3) (2006) 1116–1128.

[28] L. Breiman, Random forests, Machine Learning 45 (1) (2001) 5–32.

[29] L. Rineau, M. Yvinec, A generic software design for Delaunay refinement meshing, Computational Geometry 38 (1-2) (2007) 100–110.

[30] J. Escobar, E. Rodríguez, R. Montenegro, G. Montero, J. González-Yuste, Simultaneous untangling and smoothing of tetrahedral meshes, Computer Methods in Applied Mechanics and Engineering 192 (25) (2003) 2775–2787.

[31] A. Tagliabue, L. Dede', A. Quarteroni, Fluid dynamics of an idealized left ventricle: the extended nitsche's method for the treatment of heart valves as mixed time varying boundary conditions, MOX report 61/2015.